Lasers, lenses and light curves : adaptive optics microscopy and peculiar transiting exoplanets

Werkhoven, T.I.M.

CHAPTER 1

Introduction to adaptive optics microscopy

With vision being one of the senses, light is an important tool for studying one's surroundings. The behaviour of light has been studied extensively throughout history, ranging from Euclid in the 4th century BC to Newton's Opticks in 1704. To help in their studies, people built tools, starting with simple lenses possibly as far back as the 8th century BC with the Assyrian Nimrud lens (Layard, 1853). The invention of the telescope took place somewhere in the 16th century, but it is not clear whom is to be credited with the invention, if that is even applicable here[1]. Indeed, various names have been mentioned as inventors at different times, including persons from the Netherlands, England, France, Spain and Italy (Zuidervaart, 2010; Kriss & Kriss, 1998). The story of the first microscope is similar, also here it is unclear who *invented* the microscope. For investigation of minute objects, Dutch draper Antoni van Leeuwenhoek was one of the first to build microscopes, although others were active in this field as well, such as Robert Hooke (Bardell, 2004). Since then, both telescopes and microscopes have come a long way, with the ability to distinguish on one end dim, distant planets orbiting their host stars to on the other hand synaptic vesicles tens of nanometers in diameter (Marois et al., 2008; Kalas et al., 2008; Willig et al., 2006).

[1] Zuidervaart (2010) argues that the telescope was not *invented* per se, but was more a recognition of the capabilities of devices already in existence.

1.1 Imaging

When creating images by recording light, the quality of the image is influenced by everything the light finds on its path. This can be a human eye, imaging the letters of a newspaper on the retina, or a telescope, feeding light of extrasolar planets onto a camera. In neither case is the image perfect, people often need glasses at old age and even before, visual acuity is finite. In the latter example, besides the telescope's optics, the Earth's atmosphere is of great influence on the image quality, blurring details that would otherwise reveal important information.

One solution to this is to go to space void of atmospheric influence, and indeed many telescopes operate from space, with *Hubble Space Telescope* perhaps being one of the most well-known examples. While space-based telescopes have great advantages, they are expensive and limited in size. Another solution is to build telescopes in places where the influence of the atmosphere is minimal. Often this is on high mountains, with less atmosphere between the observer and the stars, or on an island in a lake where the surrounding water creates stable air, or in places with steady, clean wind providing a clear atmosphere. Nevertheless, even the best places on Earth suffer from artefacts which ultimately limit the resolution of ground-based telescopes. These artefacts are called *seeing*, and are due to the turbulent mixing in the atmosphere of layers with different temperatures. Because refractive index is a function of temperature, these bubbles cause refraction of the incoming light, degrading the quality when imaging (Fig. 1.1). This problem was known as early as the 19th century when people built telescopes large enough to notice the effect (Hough, 1885) and indeed people suggested methods to alleviate this to some extent (Langley, 1903), but no solution for this problem existed for a long time. The effect of seeing is not unlike the image deformation seen when looking underwater, where the wavy water surface bends the light and deforms the image of what lies underneath (Fig. 1.2).

Active correction of aberrations caused by the atmosphere is therefore necessary to allow diffraction-limited imaging from ground-based telescopes. For this reason, *adaptive optics* was developed in the fields of defence and astronomy independently, one group was trying to look up, the other was looking down. In both cases, a 20 km thick layer of turbulent air was in between the object and the observer, which required active compensation of aberrations this air created.

The technique was first publicly proposed by Babcock (1953) in the United States, and independently discovered by Linnik (1957) in the U.S.S.R. While the technique had been known, it was not until the 1980's that the

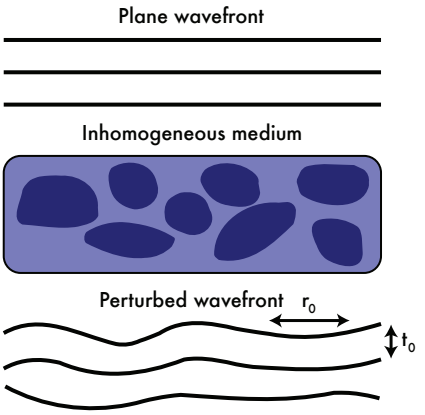

Figure 1.1: A schematic illustration of wavefront perturbation by turbid media. The plane wavefront enters at the top, traverses through the inhomogeneous medium, and comes out perturbed. The different shades in the figure illustrate differences in the index of refraction, n. r_0 and τ_0 indicate the spatial and temporal correlation of the aberration, respectively.

U.S.military built the first working adaptive optics systems at the Starfire Optical Range (SOR) in New Mexico and the Advanced Electro-Optical System (AEOS) on Maui (Reed et al., 1990; McCray, 2000). This delay was due to the computational requirements for such a system to operate, and without computers it was unfeasible. The declassification of these military systems began in 1988, with an important milestone being the AAS meeting in 1991 where the laser guide star assisted adaptive optics work was presented (Duffner, 2009).

Two decades after the declassification, adaptive optics is common on telescopes, for example on Gemini South (GPI, Macintosh et al., 2008), the Subaru Telescope (HiCIAO, Hodapp et al., 2008), and the Very Large Telescope (NACO, Lenzen et al., 2003). While many telescopes use adaptive optics, it is often implemented as an add-on system and not fully integrated in the telescope optics. This is not ideal as it requires extra optical components for sensing and correction. On the contrary, the future 40-meter class telescopes to be constructed the coming decade are designed with adaptive optics in mind, where the necessary optics will be integrated (McPherson et al., 2012; Bouchez et al., 2012; Ellerbroek, 2013).

As adaptive optics is evolving, it is finding more applications in various

Figure 1.2: A trout underwater, showing severe optical aberrations due to the non-flatness of the water surface. The light pattern on the surface are called 'caustics', and are similar to scintillation due the atmospheric turbulence (Rocca et al., 1974). The fish was not harmed during the experiment. *Photo credit: Andrew Kirk.*

fields benefiting from this development. These fields include, but are not limited to, ophthalmology (Liang et al., 1997; Roorda et al., 2002), laser writing (Mauclair et al., 2008; Jesacher et al., 2010; Čižmár et al., 2010), as well as microscopy (Hermann et al., 2004; Booth, 2007b).

1.2 Optical Aberrations

The *point spread function* (PSF) of an optical system is the image it makes of a point source. For an instrument with a circular aperture d, the PSF is an *Airy disc* (Airy, 1834) described by

$$I(x) = I_0 \left(\frac{2J_1(x)}{x} \right)^2 \tag{1.1}$$

with $x = \pi d \sin(\theta)/\lambda$, where θ is the angular position in the image, λ the wavelength, and J_1 the Bessel function of the first kind order one. This is the diffraction-limited performance of the instrument, and the first minimum of (1.1) is given by

$$\theta \approx 1.22\,\lambda/d. \tag{1.2}$$

The limit in (1.2) is a theoretical resolution of the system; if two objects are closer together than this, they cannot be distinguished[2]. This limit, known as the Rayleigh criterion, was developed by Lord Rayleigh (1902) at end of the 19th century (Hecht, 2002, Chap. 10). Around the same time, this diffraction limit in the context of optical microscopes was formulated by Helmholtz & Fripp (1876) and later by Abbe (1883), with the latter work also including empirical verification.

In the presence of aberrations, the diffraction limit is not reached and an inferior resolution is obtained. These aberrations perturbing the wavefront can either be due to the instrument itself, e.g. misalignment, or because of external factors, such as the atmosphere. Some aberrations are common and have been known since antiquity, including defocus, astigmatism, coma, or spherical aberration which can occur in the human eye, for example. To quantify these errors, they are often represented using Zernike polynomials (von Zernike, 1934; Noll, 1976). An example of instrumental aberrations is the *Hubble Space Telescope's* initial spherical aberrations due to a defect in the primary mirror (Burrows et al., 1991), which was repaired during the first service mission (Trauger et al., 1994).

While instrument aberrations are usually static and can be prevented by careful design, external factors such as aberrations due to the atmosphere are dynamic and unknown a priori. Mitigation of the latter therefore requires characterisation of the magnitude and kind of aberrations, and active correction of the changing conditions. Kolmogorov (1941a,b) describes the local structure of turbulence in fluids, a description also applicable to the behaviour of atmospheric turbulence, which describes a power spectrum of turbulence at various length scales. Later, Fried (1965) characterised the spatial frequency on the wavefront aberrations induced by turbulence with a coherence length scale r_0, the Fried parameter. r_0, typically on the order of centimetres for visible light, is the length over which a wavefront can be considered flat, and apertures larger than this will notice resolution degradation due to seeing. Other parameters that characterise the aberrations are θ_0 and f_G. The former is the angular equivalent of r_0, called the isoplanatic patch, and indicates an angular patch on the sky over which the aberrations are invariant, typically on the order of arcseconds, again for visible light (Korff et al., 1975). The latter is the Greenwood frequency and indicates the bandwidth requirement for correction of atmospheric turbulence, which was determined to be on the order of a hundred hertz, also for visible light (Greenwood, 1977). Together, these

[2] Although somewhat arbitrary, this definition is convenient and simple. As Lord Rayleigh (1902, p. 85) writes: *"This rule is convenient on account of its simplicity; and it is sufficiently accurate in view of the necessary uncertainty as to what exactly is meant by resolution."*.

parameters give a rough statistical description of the effect of atmospheric seeing on observations.

1.3 Adaptive optics

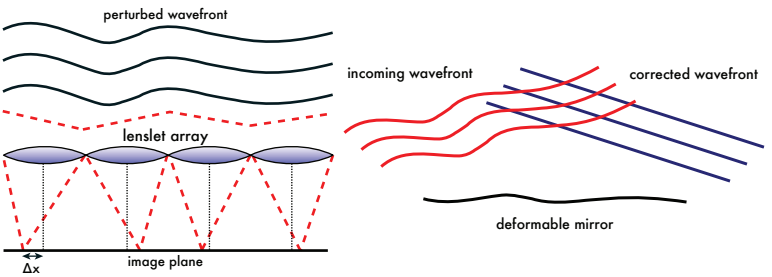

Figure 1.3: *Left:* A schematic illustration a Shack-Hartmann wavefront sensor. The telescope aperture is split up in smaller subapertures by a lenslet array. Each lens images only a part of the wavefront, such that the local phase gradient causes a displacement of the image (Δx). By measuring the spot positions one can reconstruct the wavefront. *Right:* An illustration of a deformable mirror (DM). The mirror is deformed such that after reflection the wavefront is flat.

Measuring aberrations is called wavefront sensing in adaptive optics parlance, and is the first step of correction. Because of the high frequency of visible light, there are no devices that can measure the phase of the electromagnetic wave directly, and instead all wavefront sensing devices measure the intensity of the light. Various methods exist to retrieve the phase by measuring the intensity, one common method is the Shack-Hartmann (or less common but more chronologically correct: Hartmann-Shack) wavefront sensor (Hartmann, 1900; Shack & Platt, 1971), which measures the local gradient of the phase as a displacement of a focal spot (left panel in Fig. 1.3). Using these local phase gradients the phase can be reconstructed up to a certain precision, mainly determined by the number of sub-apertures and the amount of light available. To optimally sample the aberration, the sub-apertures should be smaller than r_0 and the temporal sampling should be faster than f_G.

Once the aberration is known, the aberration is canceled by introducing the inverse shape on a correcting device with half the amplitude such that the sum of the aberration and correction yields the desired flat wavefront (right panel in Fig. 1.3). Devices to do this include deformable mirrors; a thin mirror that can be deformed using mechanical actuators, or spatial

light modulators; arrays of liquid crystals that can modify the phase. The former typically has on the order of 10 to 1000 individual actuators, and operates at speeds of kilohertz, the latter has 10^4 to 10^6 of actuators but operates at a slower rate of tens of hertz. For optimal correction the correcting device should be matched to the aberrations in both spatial and temporal resolution.

This simplified view ignores many details as various things need to be taken into account for reliable operation, including finite response speed, hysteresis, limited stroke, non-linear deformation and others. One particular issue that is becoming more important is computing power. Converting the measured aberration to actuating control is usually a matrix multiplication and therefore scales with the square of the number of degrees of freedom (typically actuators). With the number of actuators going towards the ten thousands (Kasper et al., 2010), this problem is becoming significant.

1.4 Microscopy

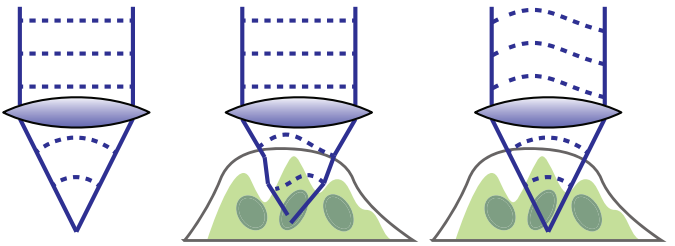

Figure 1.4: Illustration of sample-induced aberrations in microscopy. These aberrations deform the point spread function, degrading both the resolution as well as the returned fluorescence. *Left:* in absence of any aberrations, the focus is diffraction limited. *Middle:* when focussing inside a sample, the light is aberrated due to heterogeneity in the sample, giving a smeared out focus with loss of signal and resolution. *Right:* to mitigate this, one can pre-compensate the incident wavefront on the sample such that the compensation and aberration together again yield a diffraction-limited focus inside the sample. The challenge is to determine the shape to optimally compensate aberrations with.

As mentioned before, adaptive optics is also finding applications in other fields, one of these being microscopy. While it is the opposite of astronomy in terms of scale, the instruments used in both fields often deal with similar visible light, and both are affected by aberrations. When imaging with a microscope, light travels through a sample, which spatially varies

in refractive index as the Earth's atmosphere does. In Fig. 1.4 this issue is schematically illustrated. With light with similar properties, similar optics and comparable aberrations, indeed microscopy is a field where adaptive optics can be used for correction.

While the parameter space of microscopes is similar to optical telescopes (spatial, temporal, spectral resolution, field of view, collection power, etc.), there are several important differences. In microscopy, the proximity of samples under study allows illumination of those objects, and choosing the kind of illumination therefore provides a new set of parameters, such as depth penetration, contrast generation, photobleaching, and phototoxicity. Depth penetration indicates how deep light can penetrate in a sample before scattering degrades the signal and resolution significantly, and therefore how deep one can image. Contrast generation indicates that one can chemically or biologically alter a sample such that only specific parts of interest emit light when illuminated. Finally, photobleaching indicates the destruction of a dye or fluorophore, and phototoxicity describes light-induced cell death due to excessive incident laser power.

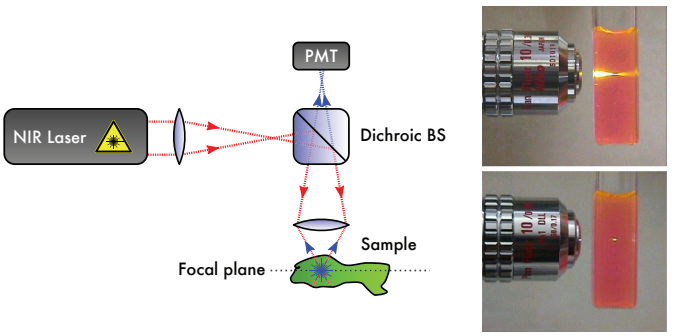

Figure 1.5: *Left:* a schematic illustration of a (multi-photon) scanning microscope. A near-infrared laser beam forms a focus inside a sample. At the focus, one or more photons to excite a fluorescent molecule which subsequently emits light at a different wavelength. This fluorescence is chromatically separated using a beamsplitter (BS) and collected by a photo multiplier tube (PMT). By moving the laser focus with respect to the sample while recording the fluorescence, an image is formed on a point-by-point basis. *Right:* comparison of single-photon fluorescence (bottom objective) and two-photon fluorescence (top), illustrating the extended emitting conical volume in the former case and the much more confined volume in the latter case due to the non-linear excitation effect. Because of the point-by-point image construction of scanning microscopes, this confinement is required to obtain axial resolution.

A specific kind of microscope is a scanning microscope, shown in Fig. 1.5, which scans the light focused by an objective through a sample (Minsky, 1961; Shotton, 1989; Pawley, 2006). The object emits light at the focus at a different wavelength, usually through fluorescence, which can be separated and subsequently collected. To form an image, the focal spot is moved with respect to the sample, either by scanning the laser beam using mirrors, or moving the sample physically with a motorized stage. By recording the fluorescence intensity as well as the location of the focus in the sample, an image is constructed in a point-by-point fashion. The resolution of such images is determined by the focal volume illuminated, which in perfect conditions is a diffraction-limited spot with lateral size

$$d \sim 0.61\,\lambda\,/\,n\sin(\theta) = 0.61\,\lambda\,/\,\mathrm{NA}, \tag{1.3}$$

with n the refractive index of the medium in which the objective is used, θ the half-angle of the objective acceptance cone and NA the numerical aperture of the objective used. For multi-photon fluorescence, where two or more photons are simultaneously absorbed to excite a fluorophore, the emitted intensity scales as $I_{\mathrm{fluor}} \propto I_{\mathrm{laser}}^{n}$, with n the number of photons absorbed. This non-linearity strongly localises the fluorescence generated to a small focal volume, creating intrinsic three-dimensional resolution (Denk et al., 1990; Zipfel et al., 2003). To obtain maximum fluorescence signal with minimal average incident power, multi-photon microscopy works best when using (sub-picosecond) pulsed lasers which deliver high instantaneous power and thus fluorescence, but low average power on the sample, thereby reducing phototoxicity.

In scanning microscopes, aberrations are caused by the sample under study perturbing the incident laser beam, among other things. While travelling through the sample towards a focus, the wavefront is aberrated, degrading the focus (Fig. 1.4 middle panel). Because the volume of the focus determines both the fluorescence intensity as well as the resolution, both quantities are degraded by these aberrations. With a spatial correlation in samples on the order of micrometers (the size of organelles in cells) aberrations become important when imaging at a depth of tens of micrometers. To solve this, one needs to pre-correct the incident laser wavefront to compensate for the sample-induced aberrations.

Adaptive optics microscopy

In scanning microscopes, it is not possible to put wavefront sensing and correcting optics in between the aberrating medium and the imaging device, as is done in telescopes. Since the aberrations occur inside the sample

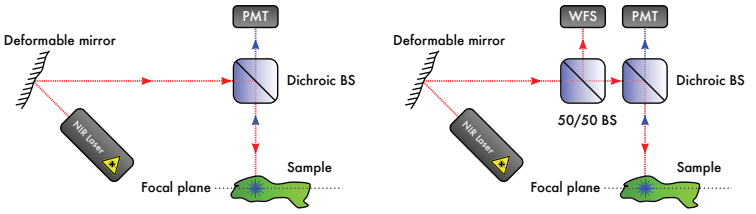

Figure 1.6: Schematic illustration of sensorless (left) and direct wavefront sensing (right) correction methods. *Left:* sensorless implementations have an extra deformable mirror compared to regular scanning microscopes. By using the fluorescence signal as optimisation metric, the deformable mirror shape can be iteratively improved, correcting aberrations. *Right:* in direct wavefront sensing additional optics direct the back-reflected laser light to the wavefront sensor (WFS). One beamsplitter (BS) transmits the fluorescence while reflecting the back-reflected laser light, the second BS directs parts of this light to the WFS. The wavefront sensor then reconstructs the aberrations, allowing direct correction with the deformable mirror.

(Fig. 1.4, right panel), the incident laser beam has to be pre-compensated such that adding the aberrations due to the specimen will yield a perfect focus inside the sample. For this reason, different wavefront sensing methods have been developed in the context of microscopy (Booth, 2007a; Booth et al., 2012), which can be divided in the following categories:

- 'Sensorless', using a proxy for the aberration such as image intensity or sharpness;
- Fluorescence wavefront sensing, measuring the wavefront off the fluorescent light;
- Direct wavefront sensing, using the backscattered laser light from the sample.

The first method has been most widely used, and uses the fluorescence intensity collected as a proxy for the aberrations (Sherman et al., 2002; Marsh et al., 2003; Booth, 2007b; Débarre et al., 2009, 2007; Facomprez et al., 2012; Tang et al., 2012). Since wavefront aberrations decrease the fluorescence intensity, the inverse implies that a maximum intensity gives a flat wavefront. Using either a model or heuristics, one can use the intensity of an image as feedback into a correction algorithm[3]. The simplest example is

[3]For an insightful illustration of various sensorless correction schemes, see Fig. 1 in Facomprez et al. (2012).

to actuate each wavefront mode on the deformable mirror sequentially, and set that mode such that the fluorescence is maximised. This method is quite robust albeit slow, typically requiring on the order of $mN + 1$ measurements, with N the degrees of freedom to be corrected and m a method-dependent factor in the range of 1 to 5.

The second method uses part of the fluorescence in a wavefront sensor (Ji et al., 2009; Azucena et al., 2010, 2011; Tao et al., 2013b, 2012, 2011b,a; Ji et al., 2011), which has some similarity to laser guide star methods in astronomical situations. One can either use autofluorescence, but because this is generally quite weak, a faster method is to use fluorescent beads injected in the sample, acting as artificial fiducial markers. The advantage is that this measures the wavefront unambiguously, instead of returning a metric that is an indirect proxy of the wavefront. The drawback is that this could require modification of the sample, and that it uses part of the fluorescence signal for wavefront sensing instead of imaging, thus requiring longer integration times for imaging or increasing phototoxicity and photobleaching.

The last method utilises the otherwise discarded back-reflected laser light for wavefront sensing (Feierabend et al., 2004; Rückel et al., 2006; Tuohy & Podoleanu, 2010; Cha et al., 2010; Wang & Podoleanu, 2012). This method combines the advantages of the former two methods, it does not use fluorescence which could otherwise be used for imaging and it provides a direct measurement of the wavefront. The disadvantage is optical complexity, as the laser light passes through the sample as well as parts of the optics twice, and selecting only the back-reflected light from the focal plane is non-trivial. Odd and even symmetry aberration modes therefore behave differently as they pass through the sample (Rückel & Denk, 2007; Booth et al., 2012; Rahman & Booth, 2013).

1.5 Current status & outlook

Astronomical adaptive optics systems are used in daily operation on various instruments, and will soon have thousands of degrees of freedom and multiple mirrors and sensors for measurement and correction (e.g. GPI (Macintosh et al., 2008), SPHERE (Beuzit et al., 2008), HiCIAO (Hodapp et al., 2008), Project 1640 (Hinkley et al., 2008)). In ophthalmology adaptive optics plays a significant role as well (Wolfing et al., 2006; Martin & Roorda, 2005; Ooto et al., 2010, 2011) and is being used in clinical applications. Compared to these fields, adaptive optics in microscopy is still in relative infancy. The different methods described above have been used by various groups over the last decade, but have focussed on development of the

technology (Booth et al., 2012). While still at an early stage, already vendors are supplying off-the-shelf adaptive optics systems for microscopy, although their scope is limited (Bifano, 2011). Despite this progress, several issues need to be addressed for adaptive optics to become as common in microscopy as it is elsewhere today. Below I discuss possible opportunities for this field in the next decade.

Aberration characterisation

While turbulence characterisation in astronomy is common, this has not been done thoroughly in microscopy. Although some studies have looked into specimen-induced aberrations in scanning microscopy (Schwertner et al., 2004a,b, 2007; Zeng et al., 2012), much work needs to be done. In scanning microscopy, the geometry of the beam is important for the aberration correction (see Fig. 1.7). When imaging deep inside a sample with relative narrow field of view, the overlap of the incident laser light beam between the two outer-most points in the field of view is significant, such that a common correction is possible for the whole field of view. Conversely, when imaging shallow or over a large field of view, one expects the aberration to be strongly position dependent, requiring new correction every time. This effect has been reported by Simmonds & Booth (2013), where the authors propose multi-conjugate adaptive optics as solution. However, before resorting to more complex solutions, it might be preferable to further characterise and validate aberration energy spectra in specimen as done in astronomy.

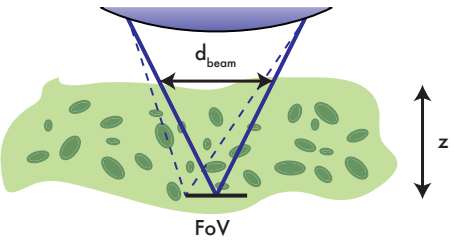

Figure 1.7: Illustration of beam and sample geometry. The focal depth z and the numerical aperture of the objective determine the beam footprint d_{beam}. Together with the typical size of refractive index variations, this determines the spatial frequency of aberrations. When scanning the beam over a field of view in the specimen (FoV, dashed lines), it samples different aberrations. The overlap between the beams determines how much the aberrations across the field of view are expected to vary, and depends on NA, depth, and the field of view.

Besides this consideration of aberration correlation-length, another important aspect is the spatial frequency of the aberrations. When imaging inside a sample, one would expect spatial frequencies on the order of $1/r_0$, where r_0 the typical length scale of the aberrations. The incident beam footprint on the sample (in air) is given by

$$d_{\text{beam}} = 2\,z\,\frac{\text{NA}}{(1-\text{NA}^2)^{0.5}}, \tag{1.4}$$

where z is the depth of the focus inside the sample and NA the objective numerical aperture (see Fig. 1.7). Combining these two quantities gives the degrees of freedom required for optimal correction of the aberrations, i.e. d_{beam}/r_0. For an imaging depth of 100 µm and an NA of 0.90, this gives a footprint of ~400 µm. With a typical size of organelles on the order of $r_0 = 1$ µm, this requires 400 correcting elements along one axis, or 400^2 in a plane. Relaxing these requirements to a depth of 50 µm with an NA of 0.75 gives a footprint of 113 µm, and taking $r_0 = 10$ µm the typical size of a cell still requires $10^2 = 100$ correcting elements. Of course this analysis does not include the relative strength of each spatial frequency contributing to the aberration, but this back-of-the-enveloped calculation is insightful to get a grasp on the requirements for correction. Modelling of these geometrical effects as initiated by Simmonds & Booth (2013) should therefore be done more extensively for better characterisation of aberrations, allowing for improved systems design and performance.

System aberrations

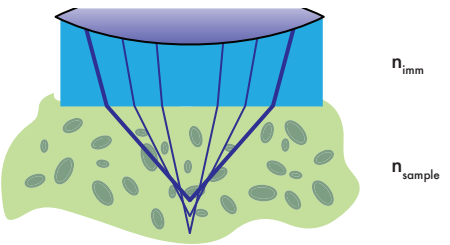

Figure 1.8: Because of the difference in refractive index between immersion fluid (n_{imm}) and the sample (n_{sample}), the converging beam suffers from spherical aberration, where focus position differs between paraxial and peripheral rays, the strength of which increases with depth. Such aberrations are not strictly due to the sample, but to a sample-system mismatch, and therefore only vary axially. The effect is exaggerated here for clarity.

There is a distinction between system and sample aberrations, where the former are due to setup misalignments, mirror non-flatness, etc. and the latter are due to the sample, as described before. Ideally, the setup used is well-aligned and delivers diffraction-limited performance. In practice, this is not always the case, which is why significant gain can already be obtained by correcting the system aberrations with adaptive optics. After correction of these system aberrations, specimen-induced aberrations can be corrected to improve the resolution further.

A kind of aberration that is a combination of these is a depth-dependent aberration due to refractive index mismatch (Hell et al., 1993; Sheppard & Török, 1997; Török et al., 1997; Booth & Wilson, 2001). Samples are usually aqueous, with a refractive index around 1.3. When focussing a beam through a plane-parallel refractive index change, this causes spherical aberration (see Fig. 1.8). For this reason water-immersion objectives are used where water is placed on the exit lens of the objective to fill the gap to the sample. Although this reduces the refractive index difference, some mismatch may remain. Because of this, there is a depth-dependent aberration that is due to the combination of objective and sample used, but not due to the fine-structure of the sample.

When correcting static system aberrations, these effects may not be taken into account. Therefore, significant improvement can be gained by correcting these aberrations in the case of considerable refractive index mismatch. Considering that this aberration only depends on depth, a single correction can be used over a large field of view at a depth z. For sample-induced aberrations a single correction would only work over a much smaller field of view where these errors are correlation, as described earlier and shown in Fig. 1.7. Indeed several papers report corrections of aberrations that only vary with depth, or use a single correction over a large field of view (Débarre et al., 2009; Jesacher et al., 2009; Olivier et al., 2009). While correction of these aberrations is required for optimal resolution, the above distinction between axially and laterally-varying aberrations is often not made in literature.

Super-resolution

With the advent of super-resolution microscopy, where optical techniques are used to obtain spatial resolution beyond the classic diffraction limit, adaptive optics can be beneficial. For example in stimulated emission depletion (STED) microscopy (Hell & Wichmann, 1994; Hell, 2003), where two beams have to overlap to within a fraction of the diffraction limit, adaptive optics can give significant advantage. In this kind of microscopy,

an excitation beam is used to illuminate a sample, where it will be excited to a fluorescent state, while a depletion beam is used to deplete excited molecules except in a confined region. To this end, the depletion beam is modulated by a phase plate to create a toroidal point spread function, such that the center of the focus has zero intensity, which is the confined region where depletion does not occur. This way only molecules in this sub-diffraction-limited volume remain excited, which will subsequently fluoresce, thus achieving a resolution better than the diffraction limit.

While regular STED microscopy uses a beam shape that is not deteriorated much by aberrations (Deng et al., 2009), this shape provides super-resolution laterally, but not axially. Using instead a π-step phase plate, also axial super-resolution can be obtained (Hell, 2003), however in this case the exact beam shape is more severely influenced by aberrations. For this reason, people are using spatial light modulators (SLMs) to optimise not only beam alignment, but also correct low-order aberrations (Kromann et al., 2012; Gould et al., 2012).

In addition, because of the sensitivity to aberrations, using STED to image deep ($\sim$ 100 µm) is possible, but challenging, and indeed these applications use low order aberration correction through an objective's correction collar (Urban et al., 2011). The potential for adaptive optics here is obvious, with a closed-loop aberration correction scheme, correction far greater than only using a correction collar can be used. This will not only help to align excitation and depletion beams, but also to alleviate aberrations deeper in the sample. Compared to regular scanning microscopy, in this application adaptive optics is almost a necessity, and a suitable field for new applications.

The next decade

Although not exhaustive, the possibilities iterated above provide some ideas on where to go in this field. Characterisation of aberrations should be the initial focus for adaptive optics microscopy, which requires reliable wavefront sensing techniques. With knowledge of aberration spectra adaptive optics systems can be tailored to correct those errors that are most detrimental for image quality. Furthermore, collaboration between different fields can be beneficial when solving common (adaptive optics-related) problems. AO for super-resolution microscopy might, for example, borrow from extreme-AO applications in astronomy, where deformable mirrors with thousands of actuators are required. In return, adaptive optics in microscopy could provide a new market for corrector devices, such that with increasing demand there will hopefully be more incentive to develop

better and cheaper deformable mirrors, benefiting all applications.

1.6 This thesis

In this thesis we implemented a direct wavefront sensing method, where we measure the aberrations from the back-scattered laser light, as well as an improved method for sensorless wavefront sensing with optimal calibration and correction.

Direct wavefront sensing

One method we have developed is a direct wavefront sensing method, where the wavefront is obtained directly from the back-reflected laser light (Chap. 3). When using the back-reflected light for wavefront sensing, one needs to select only the light that reflects back from the focal volume, and reject much stronger ghosts due to the cover glass and objective optics, for example. For this reason the direct wavefront sensing method uses a confocal pinhole and coherence gating (Feierabend et al., 2004) to suppress out of focus light.

Because the lasers used in multi-photon microscopy are pulsed, we can exploit this to use coherence gating where only light from a selected plane of interest is interfered with a reference beam. Light reflecting off different layers not arriving co-temporally with the reference beam will thus not interfere. By selecting only the light in the interference pattern, we can select the light back-reflected from a confined region in the specimen. To obtain the wavefront in a single measurement, we tilt the reference beam, generating a interference fringe pattern in the back-aperture plane of the objective (Takeda et al., 1982). The deformation of the fringe pattern encodes the wavefront aberrations. Obtaining the measurement in a single exposure improves the robustness against vibration over multi-frame wavefront sensing methods, since exposure is much shorter than the time between two consecutive frames (Rückel et al., 2006).

To measure the wavefront in a robust way, we scan the laser beam over an area while measuring the wavefront, such that artefacts such as speckles are averaged out. Additionally, we use a virtual Shack-Hartmann to smooth the retrieved phase from the fringe pattern (Rückel & Denk, 2007). This step is required because the back-reflection from the focus is not a single point but a volume of scattering point sources, where each source contributes to the interference pattern on the camera. Because these point sources are not in one plane, this creates singularities in the phase which

is problematic for phase unwrapping techniques. Using a virtual Shack-Hartmann overcomes this problem.

We implemented and verified this method successfully in a custom-built two-photon fluorescence microscope in both rat tail collagen tendons and MCF-7 cancer-cell spheroids using different objectives. We are able to correct both even and odd modes, which we interpret as the back-reflection not being purely specular which would cancel out odd aberrations due to the double-pass through the sample.

Sensorless correction

Complementary to this method, we developed a model-driven, sensorless correction scheme with robust model identification (Chap. 4). Because sensorless correction is a feedforward algorithm, the deformable mirror calibration is more important than in a closed-loop feedback system. To this end, we developed a method to construct an orthogonal set of basis modes that the deformable mirror can produce and removed modes that were poorly represented or had strong mechanical cross-coupling. Additionally, we removed the tip, tilt and defocus modes as these represent lateral and axial translations of the focal spot, and not aberrations. Since these modes cannot be detected in a sensorless system, the correction should not introduce tip, tilt and defocus, which results in undesirable translation of the image.

After obtaining a suitable basis set to drive the deformable mirror with, we developed and validated a robust method to identify the dependence of the metric on the wavefront aberrations (Antonello et al., 2012). In our case, we used the mean image intensity as the metric, which inversely scales with the square of the aberration amplitude for small aberrations (Débarre et al., 2009). Because the metric has a global maximum (i.e. the intensity is maximum in the absence of aberrations), this implies that the model used for the metric must be positive semidefinite. While acknowledged by others, their proposed methods for computation of the model did not take this into account (Débarre et al., 2008; Facomprez et al., 2012). Here we do enforce a positive semidefinite solution for the model, making the identification more robust against noise and providing a more accurate description of the metric.

To correct for sample aberrations, in model-based sensorless correction schemes one sets trial aberrations on the deformable mirror and records the corresponding metric value. Using the metric model one then computes the unknown aberration vector for each mode used for correction. Various methods have been proposed to do this, either solving the

paraboloid independently in each dimension (Débarre et al., 2007), or solving it globally, using the measurement data optimally. In this work we use a minimisation scheme to minimize the aberration globally using the minimum $N + 1$ measurements to obtain a solution.

We validated the method successfully in the same custom-built microscope on collagen tendons extracted from rat tail. The metric model identification was verified by cross-validating different calibration datasets against each other, where we found good agreement. Furthermore, we investigated the variation of the model across the specimen, which is important for the correction scheme to be used. If a model varies across the sample, either the model must be re-identified, or a more general correction scheme must be used. Although we have not performed an extensive analysis, we found indication that the model varies through the specimen.

For this chapter my contribution was the construction of the experimental setup and collaboration on the experimental validation of the identification and the correction.

Lessons learned

By implementing both direct wavefront sensing and a sensorless correction scheme for correcting aberrations, we have gained insight in best practices for construction of such systems. We briefly present these findings here as recommendations for future work.

When using a 19-actuator deformable mirror in our experiments we were limited by both stroke and number of modes. In our case we were especially constrained by the limited stroke in spherical aberration, often occurring in microscopy settings. Correcting setup aberrations therefore used a significant portion of our available stroke, limiting the efficacy of the DM in subsequent experiments. Therefore, a deformable mirror that can drive the first 40 Zernike modes, and a stroke of several radians rms for at least the first 15 Zernike modes would be preferable.

Although direct wavefront sensing provides a direct measurement for the wavefront, it can be quite noisy, especially for odd modes which have a lower sensitivity. Furthermore we found significant coupling between different Zernike modes when measuring the response of the DM through the sample; when setting a single mode on the DM, the wavefront sensor would measure not only that mode but also other modes. For example we noticed cross-talk between modes Z_5 and Z_6. This could be due to calibration issues for the deformable mirror, but we believe that there is also crosstalk between different modes due to the back-scattering in the sam-

ple. For optimal control, one would need to measure a response matrix which maps the measured modal representation of the wavefront as function of specific input aberrations set by the DM, something also mentioned in Rahman & Booth (2013).

For wavefront sensorless schemes, a simple model is perhaps the best. While theoretically optimal solutions should provide superior performance, in a laboratory-environment these assumptions can break down and do not provide significant improvement. Considering that a model might not be valid over the whole specimen, a correction scheme should be robust against this change.

In our experiments we used a piezo stage to move the sample instead of the beam. Although this is optically easier and better for implementing AO, it is probably more favourable to use scanning mirrors which have far greater bandwidth and can therefore be much faster when testing correction schemes.

The non-linear speed of a piezo stage is not an issue if position feedback is provided. Using the position feedback, the recorded fluorescence intensity can easily be remapped on a Cartesian grid. In spite of this, the limited stroke of the piezo at faster speeds does pose a problem.

Finally, we have learned it is preferable to build your own setup as opposed to using a commercial system. The ease of use these systems bring often goes hand in hand with difficulty to modify them and lack of technical documentation. Building an optical setup from scratch allows much greater control over the design which makes testing and modifying significantly easier.